



# Potential failure patterns of a large landslide complex in the Three Gorges Reservoir area

Y. Dong<sup>1,2</sup> · Z. Liao<sup>3</sup> · J. Wang<sup>4</sup> · Q. Liu<sup>4,5</sup> · L. Cui<sup>6</sup>

Received: 1 September 2022 / Accepted: 28 December 2022 / Published online: 12 January 2023  
© Springer-Verlag GmbH Germany, part of Springer Nature 2023

## Abstract

Potential catastrophic re-activations of ancient massive landslides in reservoir areas have posed serious threats to the safety of local people and the ecological environment. Failure mechanisms and subsequent sliding processes of re-activated massive landslide complexes are relatively complicated and remain to be an open issue. In this paper, the potential sliding process of the Huangtupo landslide, one of the largest ancient landslide complexes undergoing multiple stages of motion in the Three Gorges Reservoir area, is numerically investigated by the arbitrary Lagrangian–Eulerian method with an adaptive meshing technique. The shear strengths of the soils in the sliding zone are determined using the strength reduction method along with a series of laboratory experiment tests. Sensitivity analysis is performed to examine the dependence of the sliding masses upon the shear strength, which illuminates the failure modes of the sliding masses under the weakening effect of water flow upon the toes of the landslide. Then, the sliding mechanisms and the influence zones of the landslides are analysed. Results show that the failure of a retrogressive landslide is much more harmful than that of a thrust-type landslide in the multi-stage landslide events and the consequence of a landslide is more severe when the sliding masses share common sliding surfaces. The present study provides a paradigm for the assessment of the consequence of massive landslide complexes from a numerical perspective.

**Keywords** Large deformation finite element · Failure processes · Re-meshing · Landslide complex

## Introduction

The Three Gorges Reservoir, having approximately 2000 km of shoreline on the mainstream of the Yangtze River, is the largest hydraulic and hydropower engineering project in the world (Tang et al. 2015). Construction of the reservoir since 2003 has induced many new landslides in addition

to the re-activations of ancient landslides in the local geohazard-prone areas. The local government has invested tens of billions of dollars in geological disaster prevention and control, with more than 1.13 million people being forced to resettle in new residential areas. In the past 20 years, more than 725 small- and medium-sized unstable slopes have been reinforced with a variety of slope stabilisation

---

✉ Q. Liu  
qingbing@cug.edu.cn

Y. Dong  
dongyk@cug.edu.cn

Z. Liao  
liaozx@cug.edu.cn

J. Wang  
wangjinge@cug.edu.cn

L. Cui  
lcui@whrsm.ac.cn

<sup>1</sup> College of Marine Science and Technology, China University of Geosciences, 388 Lumo Road, Wuhan 430074, China

<sup>2</sup> Hubei Key Laboratory of Marine Geological Resources, China University of Geosciences, 388 Lumo Road, Wuhan 430074, China

<sup>3</sup> Key Laboratory of Geological Survey and Evaluation of Ministry of Education, China University of Geosciences, 388 Lumo Road, Wuhan 430074, China

<sup>4</sup> Badong National Observation and Research Station of Geohazards (BNORSG), China University of Geosciences, 388 Lumo Road, Wuhan 430074, China

<sup>5</sup> School of Civil, Environmental & Mining Engineering, The University of Western Australia, 35 Stirling Highway, Crawley WA6009, Australia

<sup>6</sup> State Key Laboratory of Geomechanics and Geotechnical Engineering, Institute of Rock and Soil Mechanics, Chinese Academy of Sciences, Wuhan 430071, China

works and retaining structures (Hu et al. 2019). However, for existing slow-moving landslides with massive volumes exceeding 10 million m<sup>3</sup>, such as the Qianjiangping landslide (Wang et al. 2004), the Huangtupo landslide (Cojean and Cai 2011), the Majiagou landslide (Hu et al. 2019), and the Outang landslide (Luo and Huang 2020), the currently available techniques are incapable of controlling their creep induced movements due to the very high kinematic energies. Therefore, potential catastrophic re-activation of the ancient (existing) massive landslides have posed serious threats to the safety of local people and the ecological environment of the Three Georges Reservoir area.

Existing landslides in the Three Gorges Reservoir area tend to be re-activated under the combined effects of continuous precipitation, fluctuations of the reservoir water level, bank erosion, human activities, and seismic loadings (Yin et al. 2010; Du et al. 2013; Huang et al. 2018). Relationships between the deformation characteristics and the influencing factors for the small- and medium-sized slopes were established quantitatively or qualitatively through small-strain numerical analyses (Wang et al. 2014; Xia et al. 2015; Alonso and Pinyol 2016; Song and Cui 2016; Xu and Niu 2018; Guo et al. 2023a, b) and laboratory physical modelling (Jian et al. 2009; Huang et al. 2017; Hu et al. 2019). However, there are no available prediction models or theories that are applicable to all the specific landslide cases and a clear understanding of the sliding mechanisms of newly triggered landslides and re-activation processes of ancient landslides remains challenging. Comprehensive geological investigations previously conducted indicate that a large number of the existing massive landslides in the Three Georges Reservoir area typically underwent multiple stages of movements over a relatively long term rather than a single landslide event over a very short time span. These massive landslides, or termed landslide complexes, are often composed of multiple small- and medium-sized sliding masses with distinct sliding surfaces (Yin et al. 2010; Wang et al. 2018, 2021). Monitoring data reveal that most of these landslide complexes are more prone to local failures rather than global catastrophic sliding (Tang et al. 2015). An earlier local failure may induce a series of subsequent sliding events, since the supporting conditions of the remaining slopes are undermined. Consequently, the failure mechanisms and the subsequent sliding processes of the re-activated massive landslide complexes are relatively complicated and thus have rarely been studied (Kasai et al. 2009; Della Seta et al. 2013; Young 2015).

Based on in situ monitoring of the landslide evolutions, early warning of disaster occurrences is feasible to reduce potential casualties (Yin et al. 2010; Song and Cui 2016; Fan et al. 2022). Currently, it is paramount to clarify the landslide processes and assess their consequence so that appropriate mitigation measures can be taken. In this paper,

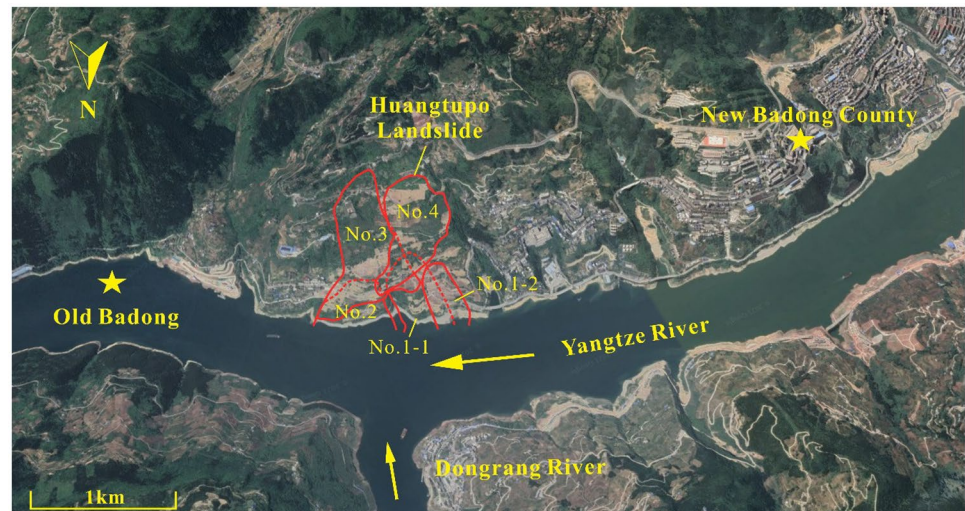
the potential sliding process of the Huangtupo landslide, one of the largest active landslide complexes in the Three Gorges Reservoir area, is investigated by using the arbitrary Lagrangian–Eulerian (ALE) method with an adaptive meshing technique. The ALE is a novel and efficient numerical method that allows the simulation of the large deformation of materials using the Lagrangian and Eulerian frameworks simultaneously. In comparison to the conventional small-deformation methods, the entangled meshes in the ALE are periodically re-constructed to derive the actual deformation of the sliding mass. In the numerical model, the average shear strengths of the soils in the sliding zone are determined using the strength reduction method (SRM) along with a series of laboratory experiments. The SRM is to assess the factor of safety associated with a slope, which is defined as the ratio of the resisting shear strength of the material to the driving shear stress developed along the failure plane. Sensitivity analysis is performed to examine the dependence of sliding masses upon the shear strength, which illuminates the progressive failure modes of the sliding masses under the weakening effect of water flow upon the toes of the sliding masses. Additionally, the potential sliding mode of the thrust type of the Huangtupo landslide is presented under stress adjustment or material softening within the rear part of the mass. Thus, the sliding mechanisms and the influence zones of the landslides are further analysed. This study provides a paradigm for the assessment of the consequence of the massive landslide complexes from a numerical perspective.

## Background of Huangtupo landslide

### Geological setting

The Huangtupo landslide is located in the new Badong County in the Three Gorges area with an axis parallel to the Yangtze River (Fig. 1). The original downtown of Badong County is below the 175-m water level since the impoundment of the Three Gorges Reservoir. The total area and volume of the whole Huangtupo landslide are 1.35 km<sup>2</sup> and nearly 70 million m<sup>3</sup>, respectively. As one of the largest and most destructive landslides in the Three Gorges area, the whole Huangtupo landslide mainly comprises four sub-landslides, namely, the No. 1 (northwest) and the No. 2 (northeast) Riverside slides, the No. 3 Garden Spot slide (southwest), and the No. 4 Transformer Station slide (southeast) (Figs. 1 and 2a). There are also numerous small-scale slides. The No. 1 sub-landslide can be further divided into two partially overlapping smaller slides, namely, the No. 1–1 and No. 1–2 slides with volumes of approximately 13 and 5 million m<sup>3</sup> and maximum thicknesses of 90 and 65 m, respectively. A field investigation conducted in 2001 found that the No. 1 and the No. 2 (20 million m<sup>3</sup>) Riverside

**Fig. 1** Location of Huangtupo landslide



sub-landslides moved before the other two sub-landslides. The toe of the No. 3 Transformer Station landslide, with a volume of 13.3 million  $m^3$ , covered the crown of the two Riverside sliding masses (Fig. 2b). The No. 4 Garden Spot landslide, with a volume of 13.5 million  $m^3$ , was the last to move and the toe of the No. 4 Garden Spot landslide covered the crowns of the No. 3 Transformer Station landslide and the No. 1 Riverside landslide (Fig. 2c). The crown elevation of the Huangtupo landslide was approximately 600 m above sea level (m.a.s.l.) while its toe varied from 50 to 90 m.a.s.l. The toe was submerged in the Yangtze River, with water levels varying from 145 to 175 m, as regulated by the Three Gorges Dam (Wang et al. 2020).

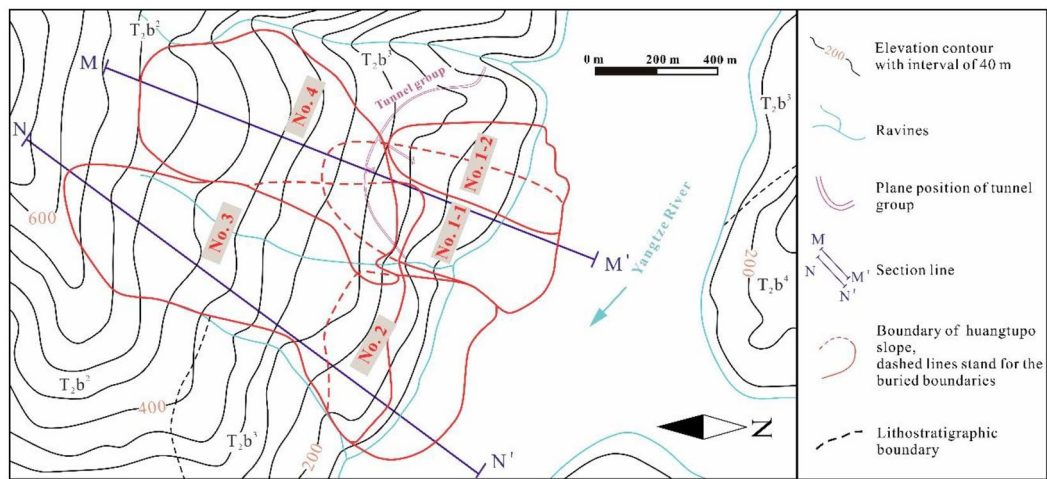
The landform of the Huangtupo landslide is polygonal-shaped, with its sliding surfaces generally along the dip direction of the underlying bedrock. Controlled by the Badong fracture–fault system, ravines were formed on the sloping surfaces along the major joints and fractures. The landslide is on a dipping stratum of the Middle Triassic Badong Formation with multiple weak layers and major rupture zones (Yu and Wu 1996; Deng et al. 2000). Multiple weak interlayers are present in the stratum of the Badong Formation. The combination of the lithology and the weak structures has induced many landslides that are sliding towards the reservoir. The weak layer is 50 cm thick, greyish-yellow in colour, and made of angular to sub-angular breccia. Sliding traces are seen at the interface between the weak layer and the overlying limestone immediately below the main rupture zones. The rupture zones are mainly composed of three lithologies, namely, brownish-yellow gravelly soil in the sliding mass, yellow and light grey clay with gravel along the sliding zone, and the cyan-brown and brownish-yellow argillaceous limestone that forms the subjacent stable bedrock. Gravel clasts with sizes ranging from 0.5 to 3.0 cm constitute about 20% of the sliding zone,

showing relatively good psephicity. The soils in the slip zone are mostly silty clay with gravel and debris, which originated from muddy limestone, and the diameter generally varies between 1 and 5 cm. Most of the gravel and debris are rounded and subangular with the particle sizes greater than 2 mm accounting for nearly 41% of the ingredients (Miao et al. 2019). More comprehensive descriptions of the Huangtupo Landslide can also be found in Tang et al. (2015).

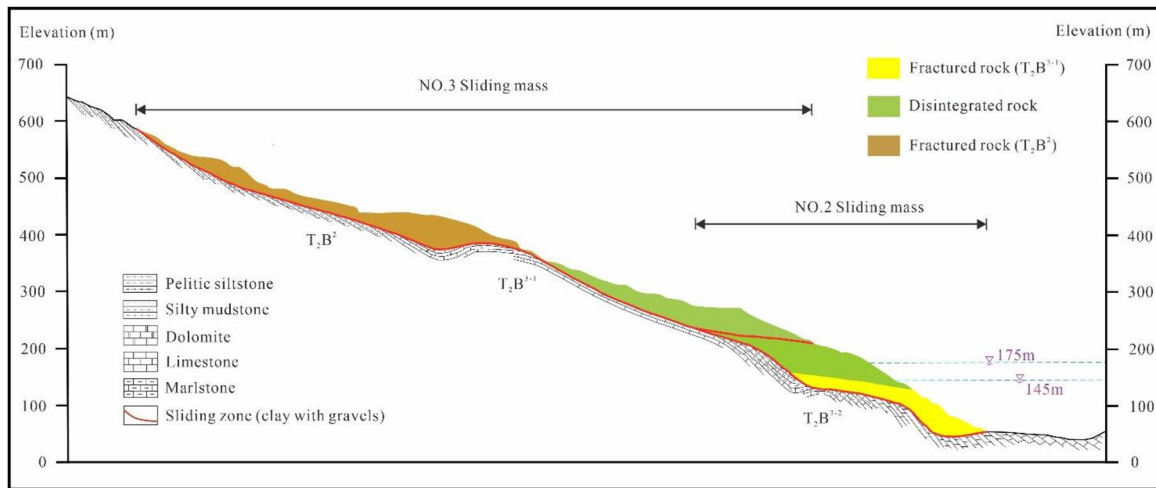
### Current movements

Among all the sliding stages, the No. 1 and the No. 2 Riverside slides are the most active ones with higher deformation rates and thus larger accumulative deformations. A ground-based interferometric synthetic aperture radar monitoring system that covered the complete landslide area was installed to monitor the deformation of the ground surface. The surface deformation at the Riverside sliding mass is shown in Fig. 3. This indicates that the largest deformation accumulated from January 2016 to December 2017 occurred in the central area of the No.1 Riverside sliding mass and it reached 9 cm.

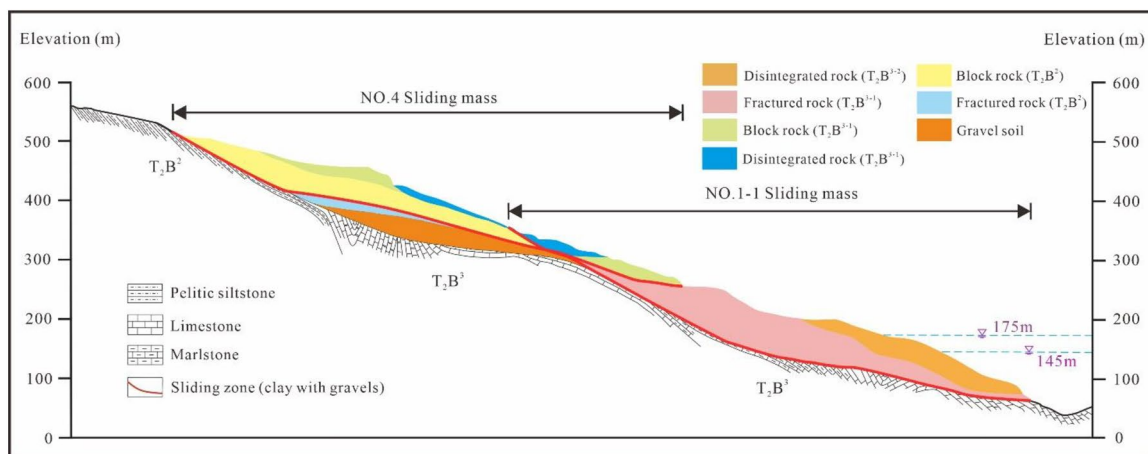
The movement of the Huangtupo landslide can be classified into two basic processes including surficial toppling and deep-seated creep. Toppling mainly occurs in the exterior part of the sliding mass and is characterised by inclination, sliding, and brittle deformation of the materials, while deep-seated creep is in the interior part and represented by ductile flows. Two sliding events in this area in 1995 were attributed to the partial re-activation mainly due to seasonal rainfalls, periodical fluctuations of the water level of the Yangtze River, and human activities, which were comprehensively investigated by Yin et al. (2010). Recent investigations using mineralogical and geochemical techniques showed that the sliding mass would be further de-stabilised as the slip-zone



(a) Multi-stages of landslides



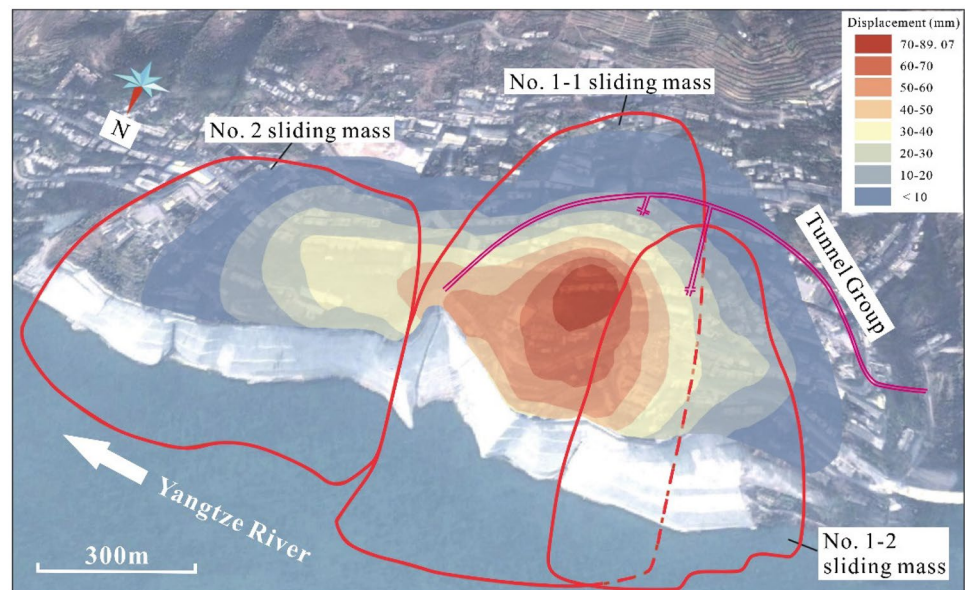
(b) Lateral view of No. 2 and No. 3 slides (N-N')



(c) Lateral view of No. 1 and No. 4 slides (M-M')

Fig. 2 Engineering geological map of Huangtupo landslide

**Fig. 3** Earth surface deformation data from January 2016 to December 2017 (the direction of displacement is towards the Yangtze River)



materials would be continuously softened by the groundwater and the bank erosion (Wen and Chen 2007). Due to the periodic water-level fluctuations, the frequent drying and wetting circles facilitate the soil structure degradation and the development/evolution of micro-cracks within the slip-zone, which represents the reduction of overall shear strength of the slip-zone materials (Tang et al. 2015; Miao et al. 2022). However, a close inspection of existing literature reveals that no research has been performed to assess the failure risk and the induced consequence of the Huangtupo landslide (Wang et al. 2021). Furthermore, the sliding mechanisms of the upper-layer No. 3 and No. 4 masses remain unclear. The insufficiency in the research of the aforementioned aspects highlights the necessity of performing numerical simulations to investigate the potential sliding process.

## Numerical modelling

### ALE method

Large deformation analysis of the sliding process of the sliding mass is needed to assess the potentially hazardous consequences of the Huangtupo landslide. The conventional continuum methods describe the movement of materials using either a Lagrangian or Eulerian mesh separately. In the Eulerian approach, governing equations are calculated in a fixed region of space where the materials are moving through a convection term. In comparison, material in the Lagrangian framework is associated with the pre-configured mesh, which seems to be more natural as deformation of the material can be directly obtained from the moving mesh. However, the Lagrangian description suffers from the disadvantage of mesh

distortion for problems with large deformations while the accuracy of the Eulerian mesh is undermined by the convection term of the material interpolated from neighbouring elements. Consequently, new formulations making full use of the advantages of both the Lagrangian and the Eulerian meshes were proposed, such as the Coupled Eulerian–Lagrangian method (Zheng et al. 2018; Zheng and Wang 2019), the ALE method (Hirt et al. 1974; Dijkstra et al. 2011; Aubram et al. 2015), the Material Point Method (MPM) (Dong et al. 2019, 2022; Dong 2020), and the Particle Finite Element Method (Yuan et al. 2020; Zhang et al. 2021). Particularly, the ALE method offers freedom on moving the computational mesh, which allows for greater distortions of the continuum than those allowed by a purely Lagrangian method, and produces results with higher resolution than those by a purely Eulerian approach (Soga et al. 2016). Therefore, the ALE method has been widely adopted in simulating the stability of slopes (Di et al. 2007) and soil-structure interactions (Nazem et al. 2009; Wang et al. 2013).

The ALE method was used in this study via a commercial software package, ABAQUS (Abaqus 2011). In the ALE method, multiple incremental steps are used in the calculation process. It should be noted that the displacements of the elements in each incremental step must be sufficiently small to avoid excessive distortions. Re-meshing of the deformed entity and mapping of the stresses and material properties from the old mesh to the new one are performed after any distortion of the mesh is detected. The new mesh needs to adapt to the contour of the domain and its typology and the connectivity must remain the same as the previous one. In the following calculations, swept meshing technique is used to generate a new mesh at each incremental step within the whole sliding mass. Note that the priority of the re-meshing

process is to improve the aspect ratios of the elements based on their current deformed positions. The new mesh is smoothed by an enhanced algorithm based on the evolving element geometry and the advection of the variables from the old mesh to the new ones is performed by second-order element centre projections.

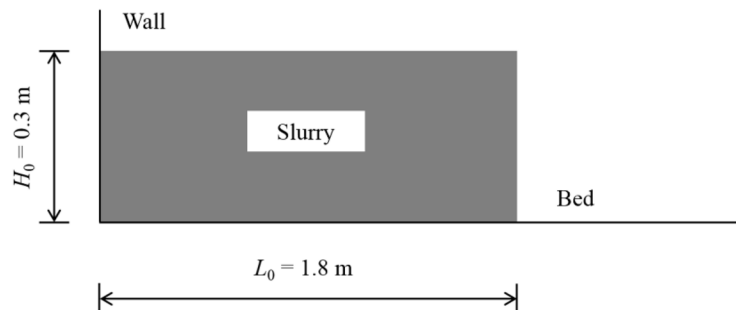
### Verification

A laboratory test of the slurry runout induced by a dam break (Krone and Wright 1987) was conducted to verify the accuracy of the ALE method. The initial configuration of the slurry sample is shown in Fig. 4a. The bed of the flume had an inclination of angle  $\theta$  of  $3.43^\circ$  relative to the horizontal. The initial length  $L_0$  and the height  $H_0$  of the slurry were

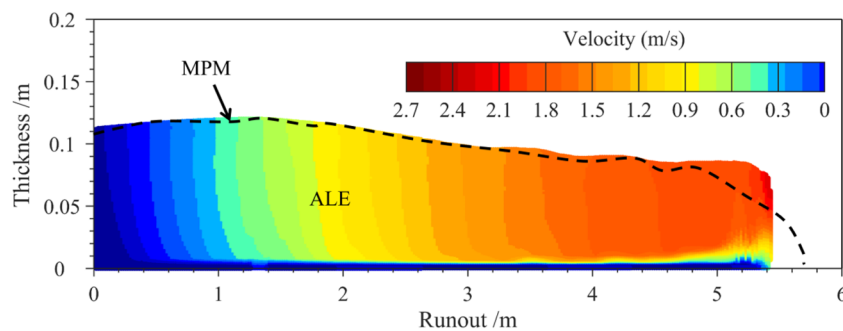
1.8 m and 0.3 m, respectively. The density  $\rho$  of the slurry was  $1073 \text{ kg/m}^3$ . The rheological behaviours of the slurry at the shear rates in the runout were approximated by a Bingham model as follows

$$s_u = s_{u0} + K\dot{\gamma} \tag{1}$$

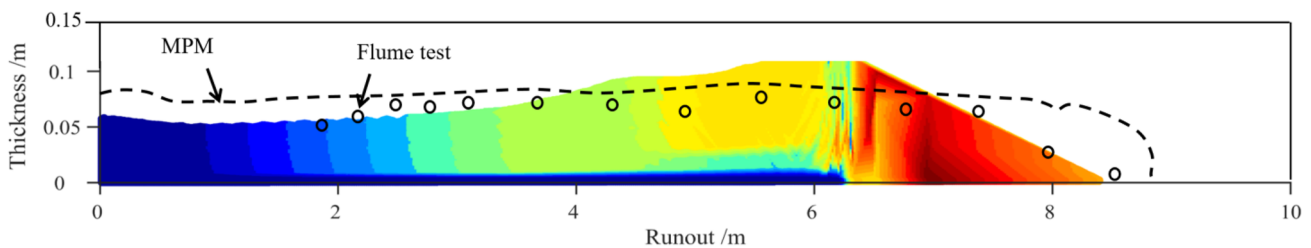
where  $s_{u0}$  is the threshold shear strength and it takes a value of 42.5 Pa,  $K$  is the consistency parameter with a value of 0.0052 Pa·s, and  $\dot{\gamma}$  is the shear strain rate. In the ALE analysis, the element size was initialised as  $H_0/20$ . The interface between the slurry and the bed and that between the slurry and the wall were described by the Coulomb friction model with a coefficient of friction of 0.5. An upper limit of  $s_{u0}$  was also imposed upon the interface shear stress to consider the shear strength of the slurry along the interface.



(a) Initial configuration of dam break (not to scale)



(b) Runout profile at 2 s



(c) Runout profile at 4.1 s

Fig. 4 Simulation of a slurry flow by dam break

The predicted runout profile at 2 s by the ALE analysis is compared with those by the MPM (Dong et al. 2019) as shown in Fig. 4b. The front head of the slurry predicted by the ALE is found to be somewhat higher than those from the MPM, which can be attributed to the friction condition along the interface between the slurry and the bed. In comparison, good agreements are observed in the tail profiles predicted by different methods. The obtained runout by the ALE analysis is close to those by other methods with a maximum difference of 6%. Therefore, the accuracy of the ALE analysis is well verified. At 4.1 s, the morphology of the slurry predicted by the ALE matches well with that derived from the flume test (Fig. 4c), although the shoulder of the slurry in the ALE result is somewhat higher. The MPM result seems to over-predict the run-out distance of the slurry. Generally, the ALE is validated to be a reliable tool to track the large deformation of sliding materials.

### Numerical model

Based on the surface digital elevation model and the spatial distribution model of the sliding surfaces obtained from previous geological surveys, monitoring, and drilling data (Fig. 5), a three-dimensional numerical model of the Huangtupo landslide was created for subsequent analyses. The width and length of the model were 2785 m along the sliding direction and about 2250 m along the strike of the landslide, respectively. The elevation of the model ranged from  $-300$  to 810 m. According to the lithology and the geological structures of the Huangtupo landslide, the whole model was divided into five groups of sliding masses and bedrocks. A main sliding surface is termed as the interface between a sliding mass and the underlying bedrock. Particularly, the upper sliding surface is the contact surface between the No. 3 and the No. 4 sliding masses and the bedrock while the lower one is the contact face between the No. 1 and the No. 2 sliding masses and the bedrock (Fig. 6). Considering that the thicknesses of the sliding surfaces were too small compared with the dimensions of the sliding masses, the sliding surfaces were simplified as contact interfaces between the sliding masses and the bedrocks. The pre-processing program HYPERMESH was utilised to mesh the numerical model by using linear tetrahedral elements. The meshing details of the sliding masses and the bedrock are presented in Table 1. Convergence studies showed that a mesh with 182,187 tetrahedral elements and 42,110 element nodes in the model were sufficiently fine, through trial cases, for assessing the stability of the slopes and their sliding distance after failure, which would be detailed later in this study (Fig. 6). The numerical analysis was performed using a total stress approach based on the dynamic explicit algorithm. The sliding masses were

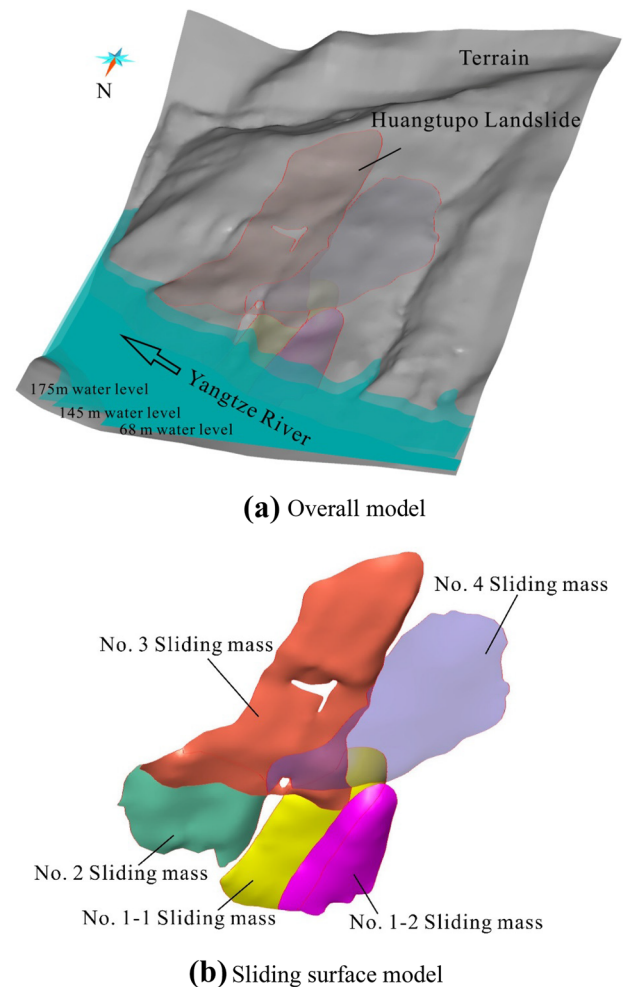


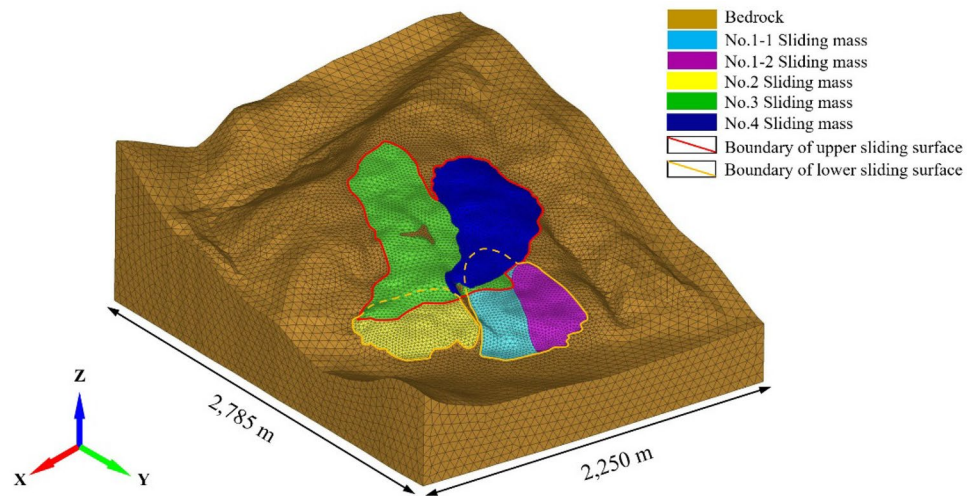
Fig. 5 Three-dimensional model of the Huangtupo landslide

modelled as elastic-perfectly plastic materials based on the Mohr–Coulomb yield criterion. The time increment was determined through the Courant–Friedrichs–Lewy stability condition. Normal constraints were imposed on the lateral boundaries of the model while the displacements along the bottom boundary were constrained in all directions.

### Parameter analysis

Properties of the sliding masses, the bedrock, and the sliding surfaces in-between are obtained from in situ and in-laboratory tests and shown in Table 2, where  $\gamma$  is the apparent weight,  $E$  is the Young's modulus,  $\mu$  is the Poisson's ratio,  $c$  is the cohesion, and  $\varphi$  is the friction angle. Particularly, the properties of the bedrock and the sliding masses were obtained from the retrieved samples by tri-axial compression tests in laboratory (Wang et al. 2021), and the range of initial shear strength parameters of the main

**Fig. 6** Mesh generation for Huangtupo landslide



sliding surfaces (or sliding zone) was directly obtained from numerous in situ shear test during tunnelling (Wang et al. 2018). A back analysis was then performed to determine the average strength parameters on the sliding surfaces as the sampling of the soil and the laboratory tests only represented a small part of the entire slip surface of the landslide. The water level in the reservoir area was considered to have a constant value of 175 m, which was the highest value throughout a year. The materials above the water level were considered natural while those below the water level were treated as saturated. After the shear failure of the soil in the sliding zone, the strength of the sliding surfaces was reduced to the residual strength, i.e. the friction angle and cohesion were  $14^\circ$  and 0 kPa, respectively, as determined by averaging the results from the in-situ tests.

Based on the surface deformation contour at the Riverside sliding masses obtained in 2017 (Fig. 3), the stability of the No. 1 and the No. 2 sliding masses was assessed by a series of studies and classified as under-stable and basically stable, respectively (Tang et al. 2015; Tomás

et al. 2016). According to the national code for geological investigation of landslide prevention GB T 32864–2016 (2016), stability factors  $F_s$  are quantified for different steady states of slopes as  $F_s < 1$ , unstable;  $1 \leq F_s < 1.05$ , under-stable;  $1.05 \leq F_s < 1.15$ , basically stable; and  $1.15 \leq F_s$ , stable. The landslide stability factors were estimated based on an interval maximum value, which was set to 1.05 and 1.15 for the No. 1 and the No. 2 sliding masses, respectively, taking conservative factors into account. Therefore, the average strength parameters on the lower sliding surface were reversely calculated based on the estimated stability factors of the Riverside sliding masses. As for the upper sliding surface, its strength parameters were directly determined from the laboratory tests since the stability information for the No. 3 and the No. 4 sliding masses are unavailable.

The SRM was incorporated in the FE program. The stability of the No. 1 and the No. 2 sliding masses was experimented with the trial strength parameters of the lower sliding surface reduced from the values ( $c$  and  $\phi$ ) obtained in laboratory tests by a series of reduction factors  $F_r$ . In the numerical simulation, at the time when the sliding masses started to fail, the corresponding strength parameters of the lower sliding surface were termed as the critical soil strength parameters ( $c_c$  and  $\phi_c$ ) and the corresponding reduction factor  $F_r$  was considered as the global factor of safety for the sliding masses.

Three types of criteria are often utilised in the reverse analysis with the SRM: (i) non-convergence in the computing process (Zienkiewicz et al. 1975); (ii) development of the plasticity zone from the toe to the top of the slope (Matsui and San 1992); (iii) a sudden increase in the displacement at the toe of the slope (Griffiths and Lane 1999). Due to the re-meshing technique adopted in the large deformation analysis, the numerical calculation process can always be

**Table 1** The meshing configurations of the ALE model

Mesh region	Elements number	Nodes number	Mesh size (m)
No. 1–1 Sliding mass	6998	2035	20
No. 1–2 Sliding mass	4425	1336	20
No. 2 Sliding mass	3269	1027	25
No. 3 Sliding mass	13591	4326	18
No. 4 Sliding mass	8913	2878	18
Bedrock	144867	30453	60



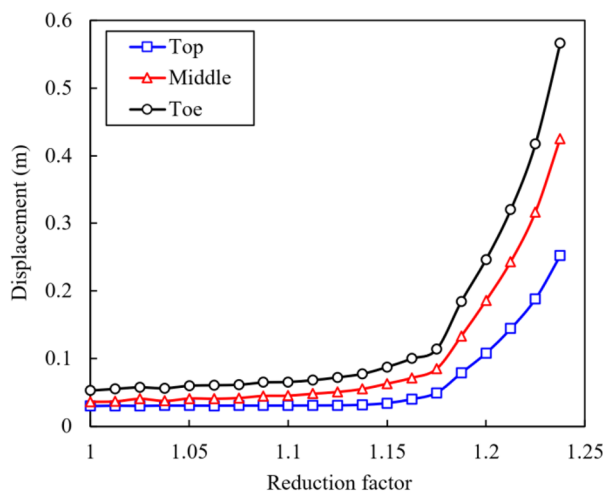
**Table 2** Properties for the materials and contact interfaces

Structure	Status	$E$ (MPa)	$\mu$	$\gamma$ (kN/m <sup>3</sup> )	$c$ (kPa)	$\varphi$ (°)
No. 1–1 Sliding mass	Natural	1560	0.31	23	130	29
	Saturated	1270	0.30	25	80	27
No. 1–2 Sliding mass	Natural	1200	0.30	21	120	28
	Saturated	960	0.29	23	70	26
No. 2 Sliding mass	Natural	2100	0.28	21	160	33
	Saturated	1720	0.28	22	120	32
No. 3 Sliding mass	Natural	1210	0.32	23	70	31
No. 4 Sliding mass	Natural	1350	0.39	27	100	27
Lower sliding surface					5~15	14~25
Upper sliding surface					35	19
Sliding surfaces (residual)					0	14
Bedrock		36,740	0.26	26	380	44

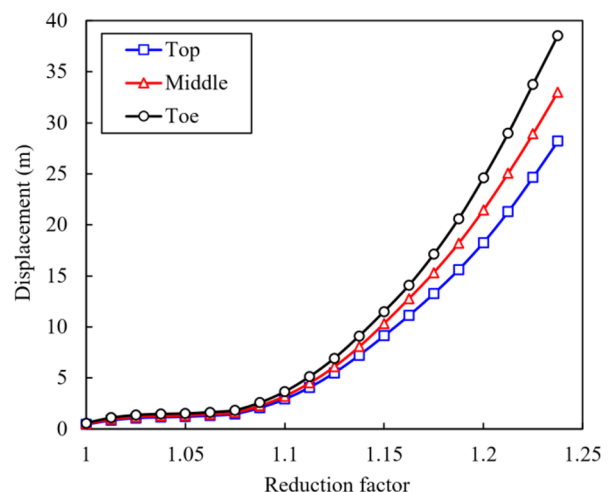
convergent throughout the calculations. Therefore, the slope failure cannot be determined by the non-convergence criterion (i). Instead, the criterion (iii) of a sudden increase in the displacement seems more reasonable as the nodal displacements within the mesh increase significantly when the slope failure occurs, which can be determined by the inflection point on the curve of displacement versus the shear strength reduction factor  $F_r$  (Fig. 7).

The nodal displacements of the Riverside sliding masses were obtained by the SRM with an increase in the reduction factor  $F_r$ , in which the representative nodes were located at the top, middle, and toe of the sliding masses (Fig. 7). It can

be found that a sudden increase in the nodal displacement for the No. 1 and the No. 2 sliding masses occurs when the reduction factors increase to 1.075 and 1.175, respectively. Therefore, the overall stability factors  $F_s$  of the two sliding masses are taken as 1.075 and 1.175, matching the values recommended by the national code GB T 32864–2016 (2016). The critical shear strength parameters of the soils in the sliding surface are then derived as  $\varphi_c = 15.46^\circ$  and  $c_c = 8.51$  kPa below the No. 1 sliding mass and  $\varphi_c = 16.82^\circ$  and  $c_c = 9.3$  kPa below the No. 2 sliding mass. The average strength parameters of the lower sliding surface ruled by the actual slope stability are expressed as  $\tan\varphi = \tan\varphi_c F_s$  and



(a) No. 1 Sliding mass



(b) No. 2 Sliding mass

**Fig. 7** Displacement profiles for riverside slides

$c = c_c F_s$ , making  $\varphi = 16.19^\circ$  and  $c = 8.94$  kPa below the No. 1 sliding mass and  $\varphi = 19.17^\circ$  and  $c = 10.70$  kPa below the No. 2 sliding mass. The derived strength parameters are within the variation range provided in Table 2 from the laboratory tests and are employed in the following analysis.

## Consequences of failure

### Failure initiation

The Huangtupo landslide is a typical reservoir bank landslide, which is subjected to severe water-induced deterioration. The soils close to the reservoir banks gradually degrade due to the periodic fluctuations of the water level between 145 and 175 m, resulting in drying and wetting cycles and thus continuous creep. The relationship between water inundation and the decrease of shear strength parameters has been described in many existing studies, e.g. Chen et al. (2016) and Wang et al. (2021), in different manners. Herein, the reduction factors for strength parameters were adopted following the method reported by Wang et al. (2021). To explore the evolution of the sliding process of the Huangtupo landslide under the influence of water-induced deterioration, the strength parameters (i.e.  $c$  and  $\varphi$ ) of the No. 1 and the No. 2 sliding masses and their sliding surfaces under the 175-m water level were incrementally reduced from the initial values while the components above the 175-m water level were unchanged. The maximum displacements of the No. 1 and the No. 2 sliding masses were obtained from the numerical analysis, as shown in Fig. 8. For the No. 1 sliding mass, the landslide deformation is less than 3.2 m when the strength parameters are reduced to 92% of the initial values, which sharply increases to approximately 13 m with the strength parameters further reduced to 89%. It implies

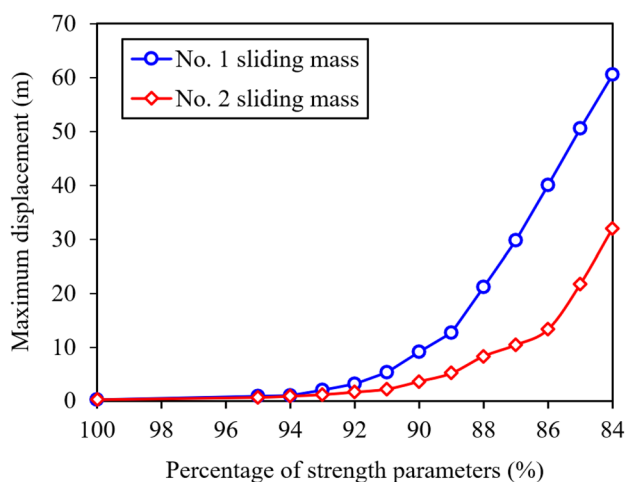


Fig. 8 Maximum displacements with different shear strengths

that the No. 1 sliding mass has suffered a catastrophic failure with the strength parameters reduced to 89% according to the failure criterion (iii) of a sudden increase in displacement. Similarly, there is an abrupt increase in the displacement of the No. 2 sliding mass when the strength parameters are decreased to 86% of the initial values, which can also be treated as a catastrophic failure.

### Sequential sliding process

The residual strength of soils is often defined as the minimum and constant shear strength at which a soil experiences a large shear displacement under a given normal stress. It occurs for slip zone soils where the shape of the particles that make up the soil become aligned during shearing (forming a slickenside), resulting in reduced resistance to continued shearing (further strain softening). In actual scenarios, the strength parameters of a sliding surface often reduce to the residual values at the initiation of failures due to the abrasion and the softening of the materials within the interface. The residual shear strength is a crucial parameter in evaluating the stability of pre-existing slip surfaces in the existing slow-moving landslides. Herein, the strength parameters of the lower sliding surfaces were set as their residual values to investigate the deformation characteristics of the sliding masses after failure. The No. 1 mass was mobilised before the No. 2 counterpart due to its lower stability factor. The whole sliding process of each sliding mass was divided into two phases, i.e. before-the-failure and after-the-failure. At the before-the-failure stage, the strength parameters of the sliding mass were decreased to the critical state values. At the after-the-failure stage, the strength parameters of the corresponding sliding surface were reduced to the residual values. Therefore, the analysis procedures were arranged

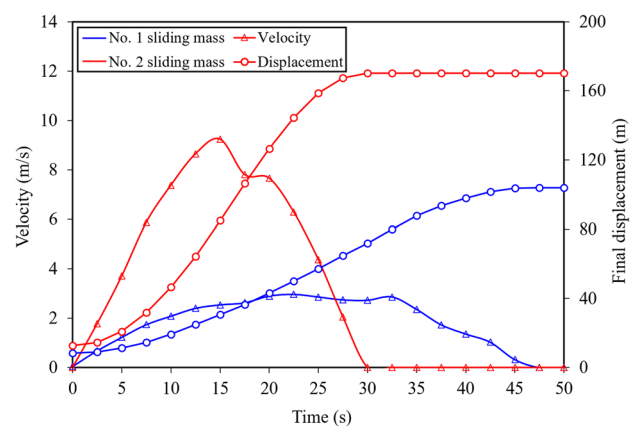


Fig. 9 Velocity and displacement history of sliding masses since failure

as follows: (i) 0~20 s, the strength parameters of the No. 1 sliding mass and its sliding surface below the 175-m water level were reduced to 89% of the initial values, simulating the creep process of the No. 1 sliding mass before failure; (ii) 20~70 s, the strength parameters of the sliding surface were set to their residual values to simulate the sliding process of the No. 1 sliding mass after failure; (iii) 70~90 s, the strength parameters of the No. 2 sliding mass and its sliding surface below the 175-m water level were reduced to 86% after the No. 1 sliding mass stopped sliding; (iv) 90~140 s, the strength parameters of the sliding surface of the No. 2 sliding mass were set to their residual values to simulate the sliding process of the No. 2 sliding mass after failure. The whole movement processes are generally very short, lasting for 50 s for the No. 1 mass and 30 s for the No. 2 mass (Fig. 9). The maximum velocity of the No. 2 mass is 9.25 m/s at 15 s, which is almost threefold that of the No. 1 mass with a value of 2.97 m/s. As a result, the

final run-out distance for the No. 2 mass is 175 m, much longer than that of the No. 1 mass with a value of 105 m. These hint that the failure of the No. 2 mass is of higher mobility than that of the No. 1 mass, although the No. 1 mass tends to fail at an earlier time.

The movement of the No. 1 mass within the first 20 s at step (i) is identical to what has been described in the ‘Failure initiation’ section. The velocity and displacement profiles of the No. 1 mass at different moments at step (ii) are shown in Figs. 10 and 11. When the sliding starts, the toe of the No. 1 mass loses its stability with the gravitational potential energy converted into the kinetic energy rapidly and then the mass is accelerated along the sliding surface under self-weight. A maximum velocity of 2.97 m/s occurs at the overlapping area between the No. 1–1 and the No. 1–2 of the sliding mass. At the end of the sliding, the volume of the No. 1 mass falling into the waterway of the reservoir area is approximately 9.39 million m<sup>3</sup>. Similar catastrophic events

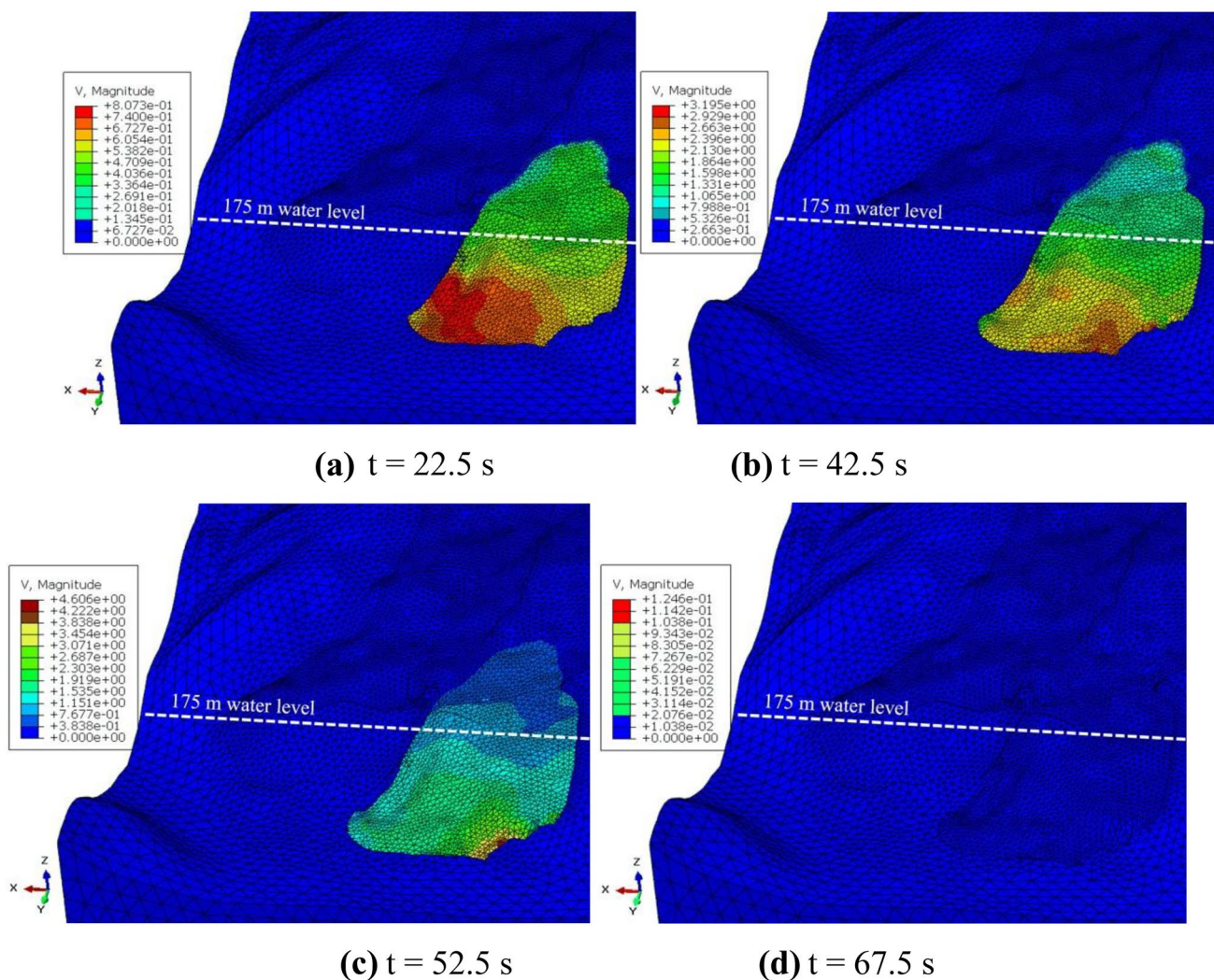
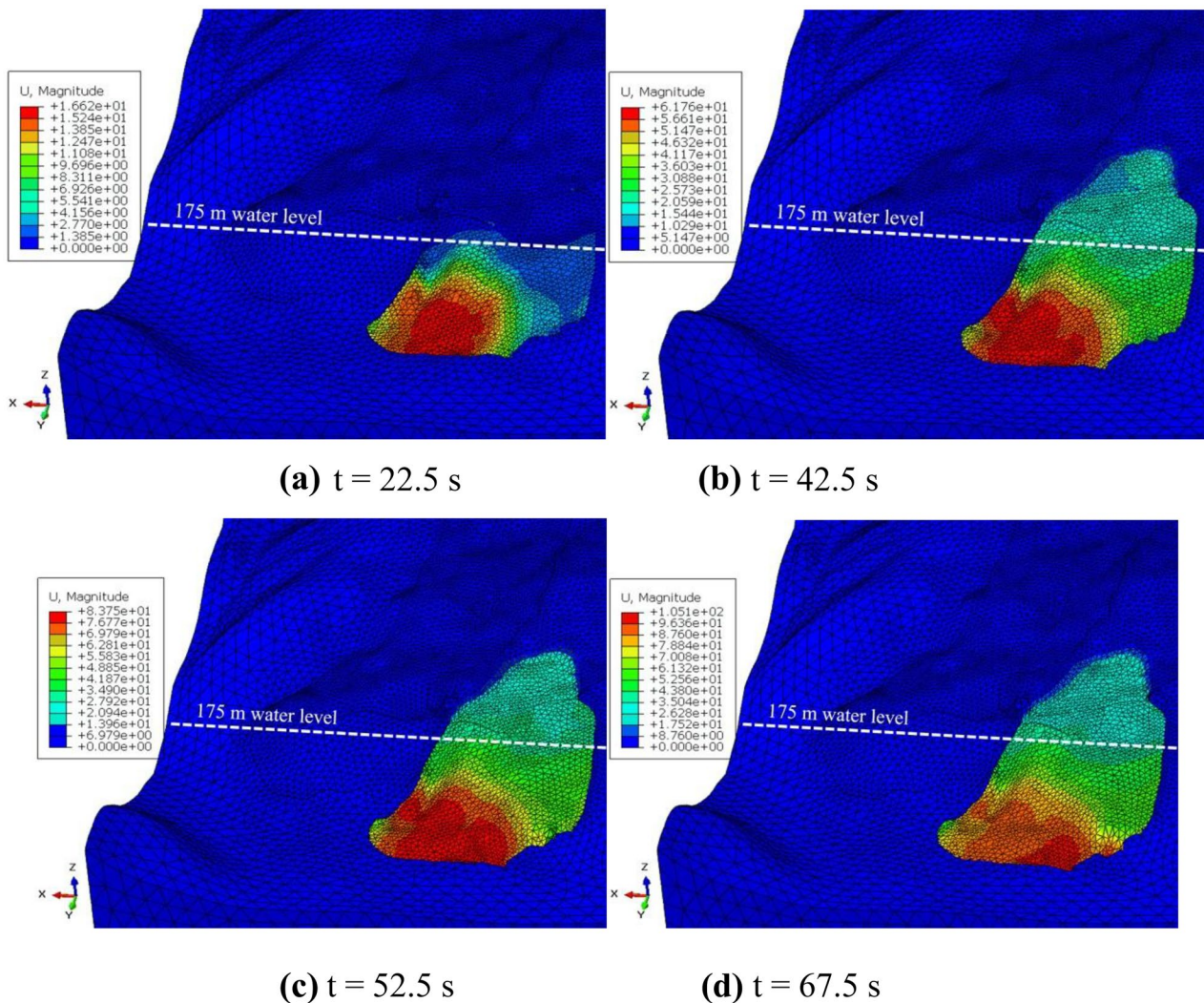


Fig. 10 Velocity contour for the No. 1 sliding mass (unit: m/s)



**Fig. 11** Displacement contour for the No. 1 sliding mass (unit: m)

were witnessed in the Three Gorges Reservoir area, such as the Qianjiangping landslide, which occurred in July 2003. During the Qianjiangping landslide, a rock mass with a value of 24 million  $\text{m}^3$  and a width of more than 250 m slid into the river, resulting in 24 deaths and 346 destroyed houses (Wang et al. 2004). The sliding of the No. 1 mass appears not to induce a further chain of disasters for its neighbouring masses as no obvious movement is detected within the No. 2, the No. 3, and the No. 4 masses in the process.

The movement of the No. 2 mass at the period 70~90 s at step (iii) is similar to what has been described in the ‘Failure initiation’ section along with slight interactions within the remaining part of the No. 1 mass. The velocity and displacement profiles of the No. 2 mass at different moments at step (iii) are shown in Figs. 12 and 13. More attention is paid to the velocities and displacements of the right-hand side of the No. 2 sliding mass, which flows

over the relic of the No. 1 sliding mass at 112.5 s after failure and stops finally at 120 s. The volume of the No. 2 sliding mass falling into the waterway of the reservoir area (below 175-m water level) is approximately 9.18 million  $\text{m}^3$ , which is close to that of the No. 1 sliding mass at analysis step (ii). Similarly, more attention is paid to the displacements of the front parts of the No. 3 and the No. 4 masses induced by the collapse of the two riverside masses (Fig. 14), which cover the rear parts of the relics of the No. 1 and the No. 2 sliding masses. The front parts of the No. 3 and No. 4 masses present obvious characteristics of extensional deformation, implying that they are dragged down by the No. 1 and the No. 2 masses (Fig. 15). In contrast, the displacements of the middle and the rear parts of the No. 3 and the No. 4 masses are very small with an order of magnitude of millimetres, showing that they are very stable in the whole process.

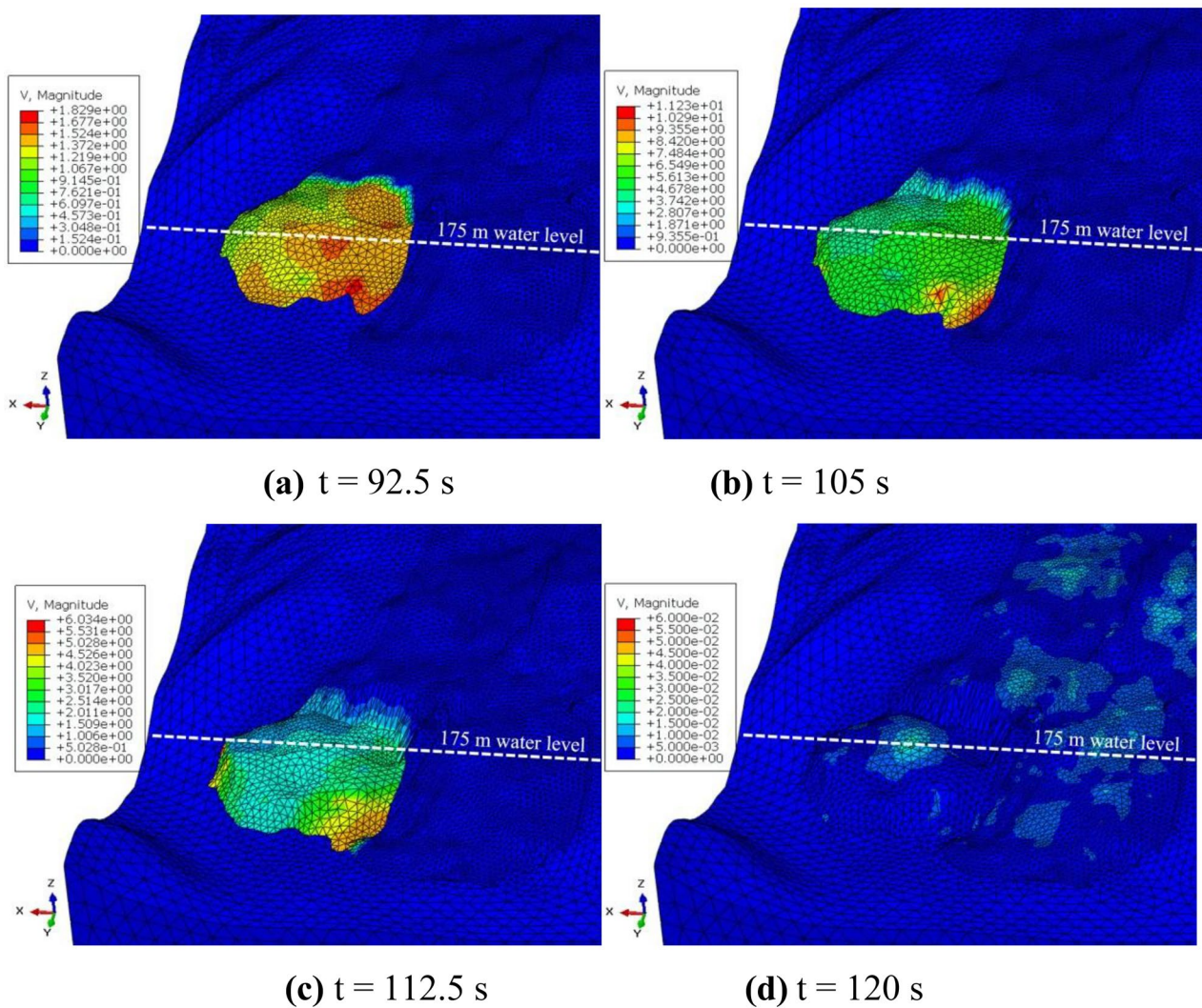


Fig. 12 Velocity contour for the No. 2 sliding mass (unit: m/s)

### Influence on the stability of neighbouring masses

It has been a major concern among the engineering geologists whether the failures of the No. 1 and the No. 2 masses of the Huangtupo landslide could weaken the stability of their neighbouring upper No. 3 and No. 4 masses, which is critical to the decision-making by the local authority with respect to disaster mitigation measures. Therefore, the stability of the No. 3 and the No. 4 masses was further assessed using the SRM during the run-out processes of the No. 1 and the No. 2 masses. The real-time deformed materials of the whole landslide (i.e. the No. 2, the No. 3, and the No. 4 masses) at different points in time were extracted from the FE model developed in the ‘[Sequential sliding process](#)’ section, based on which the stability factors for the No. 3 and the No. 4 masses were derived with the SRM analysis (Fig. 16). It can be seen that the stability of the No.3 sliding mass varies between 1.75 and

1.8, stability indicating that the local deformation at the toe of the slope does not reduce the overall stability of sliding mass. However, the time-varying stability coefficients of the No. 4 sliding mass show a ‘V-shaped’ pattern, which decrease from 1.62 to 1.49 and then increase to 1.58. Therefore, it implies that the failures of the two riverside sliding masses will not lead to the overall collapse of the Huangtupo landslide, although local deformation in the overlaying leading edge of the No. 3 and the No. 4 sliding masses will be inevitable.

### Failure mechanisms of the multi-stage sliding

In previous research on the failure patterns of the Huangtupo landslide, the failures of the No. 1 and the No. 2 sliding masses were generally considered to be caused by the

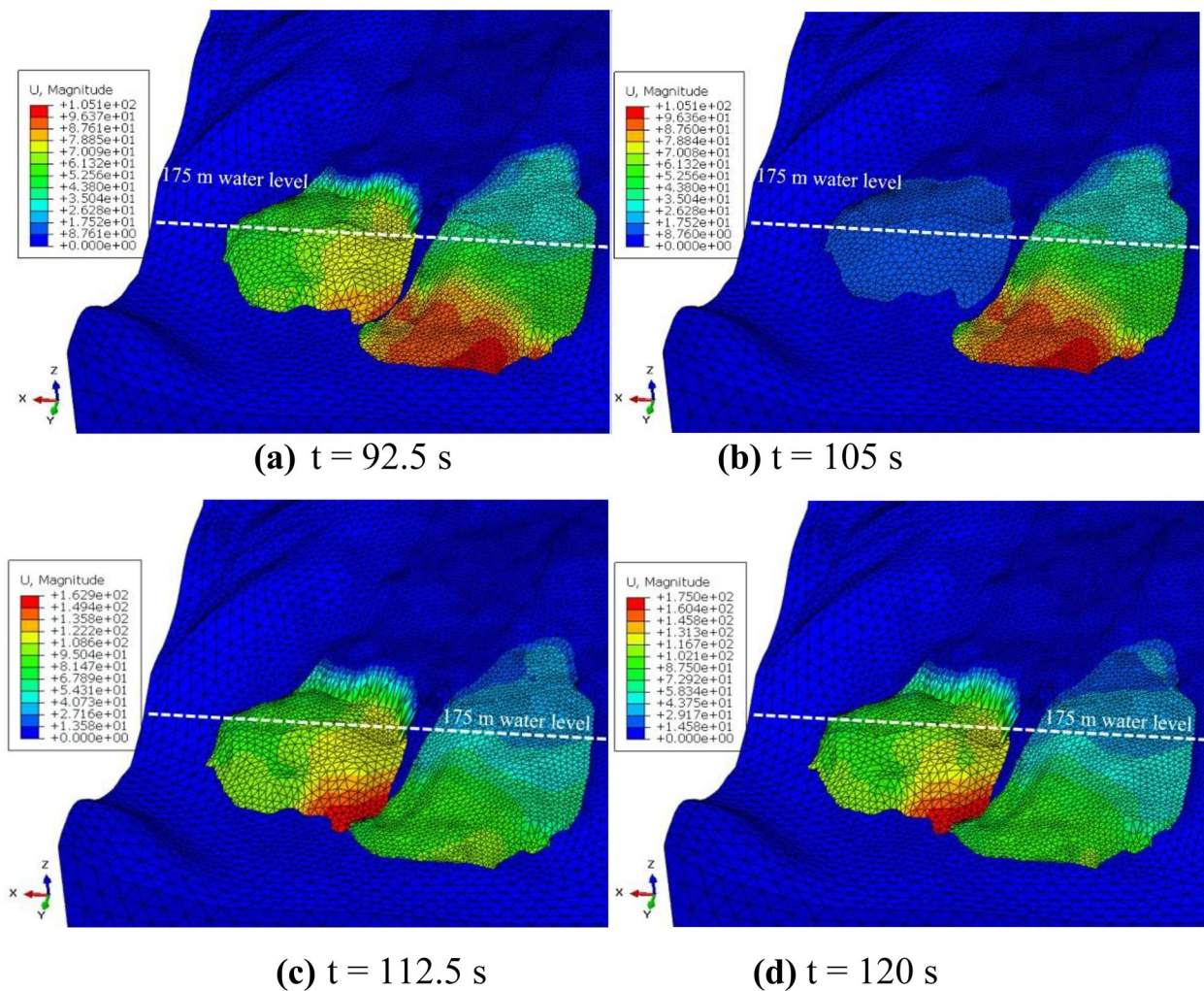


**Fig. 13** Displacement contour for the No. 2 sliding mass (unit: m)

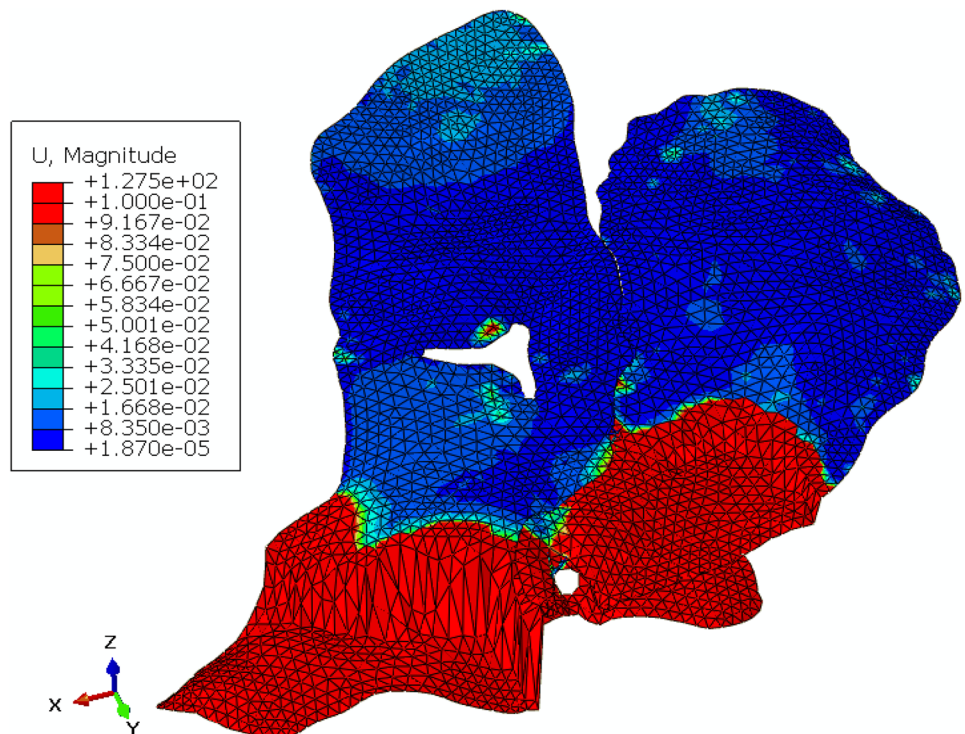
effects of water level fluctuations and toe erosion, resulting in a greater probability of a retrogressive landslide. However, there is also the possibility that the upper No. 3 and the No. 4 sliding masses would fail and slide first due to the stress adjustment or material softening within the rear part of the mass caused by overload or rainfall infiltration, respectively. Thus, a thrust-type landslide, i.e. it fails gradually from the rear part to the frontal part under the surcharge at the rear part, could be formed in this area, which could be similar to the failure of the Goleta landslide complex (Greene et al. 2008). Inspired by the two probable failure modes of the Huangtupo landslide, the landslides in reservoir areas are considered to be divided into retrogressive and thrust types in this study. In the real scenarios of the multi-stage landslide complex, the mutual interactions among the sub-landslides are quite complicated, for which the sliding modes and the sliding surface they bypass play important roles in the final sliding scales. Therefore, additional cases were calculated to

consider the influence of the sliding modes and the sliding surfaces based on representative two-dimensional profiles of the No. 2 and the No. 3 masses as extracted from the whole Huangtupo landslide model (Fig. 17), which represent the scenarios of shared and separate sliding surfaces, respectively. In the representative models, the properties of the sliding masses took the values of the No. 3 sliding mass given in Table 1 and the strength parameters for the sliding surfaces were identical to those for the upper sliding surface. Other settings, such as the step size, the mesh configuration, and the boundary conditions, in the model were similar to those in the above three-dimensional model as discussed in ‘Numerical Model’ section.

### Shared and separate sliding surfaces

The first case is for the two sliding masses with separate sliding surfaces in the representative model. A progressive

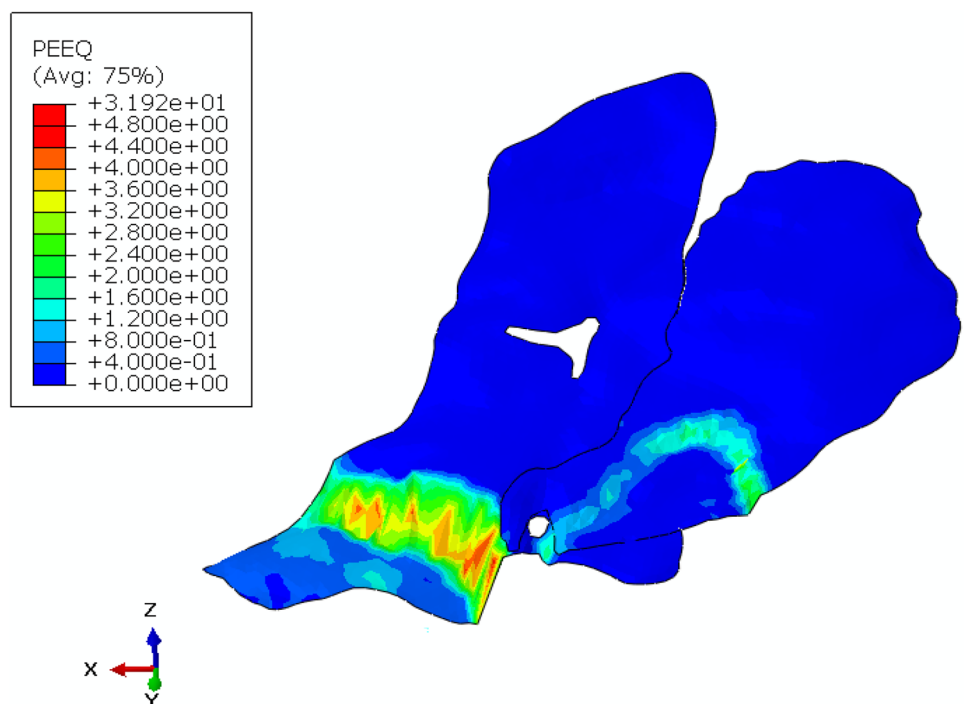
**Fig. 14** Displacement contour for the No. 3 and No. 4 landslide masses (unit: m)



failure was implemented by mobilising the lower sliding mass initially. The shear strength of the interface between the lower sliding mass and the bedrock was reduced to the residual shear strength to consider the effects of water level fluctuations and toe erosion as encountered in the Huangtupo landslide. It can be seen from the numerical analysis

that a small part of the upper sliding mass that overlaps the rear scarp of the lower mass is dragged down by the lower sliding mass while the main part of the upper mass remains un-disturbed (Fig. 18a). The final runout distance of the lower sliding mass is about 379 m. When the sliding stops, the deformed materials of the upper sliding mass are

**Fig. 15** Distribution of plastic strains in the No. 3 and No. 4 landslide masses



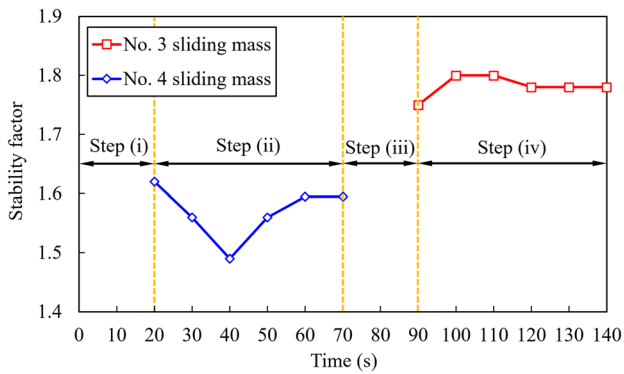
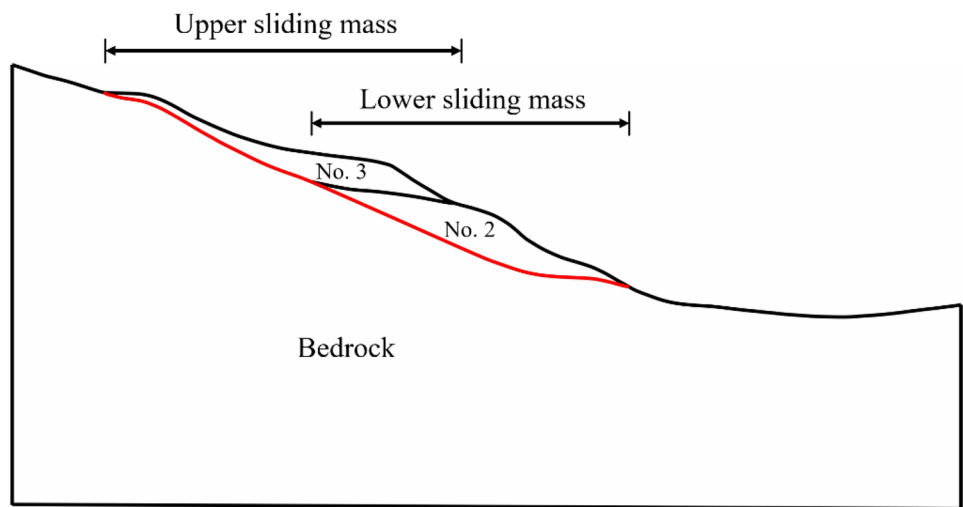


**Fig. 16** Stability factor history for the No. 3 and No. 4 landslide masses

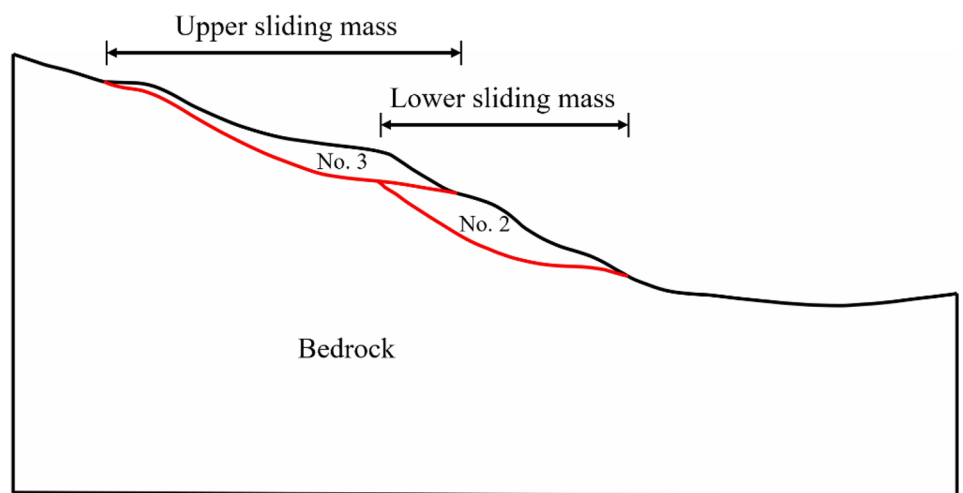
extracted into the SRM analysis. The maximum displacements of the mass under different strength reduction factors are shown in Fig. 19, indicating that the safety factor of this

area is about 1.7. Therefore, the upper sliding mass is in a state of completely stable, which is basically consistent with the Huangtupo landslide in the ‘*Sequential sliding process*’ section. The result implies that for multi-stage landslides with separate sliding surfaces, the collapse of the lower sliding mass will not necessarily cause failure of the whole upper sliding mass. In comparison, for the two sliding masses with a shared sliding surface, the failure of the lower sliding mass directly leads to a successive overall sliding of the adjacent upper sliding mass (Fig. 18b). The reason is that the support of the upper sliding mass has been removed along with the collapse of the lower mass. The final runout distance of the lower slide mass is up to 430 m. It indicates that after the failure of the lower sliding mass, whether the upper and the lower sliding masses share a sliding surface is an important basis for the overall sliding of multi-stage landslides.

**Fig. 17** Two-dimensional sliding model



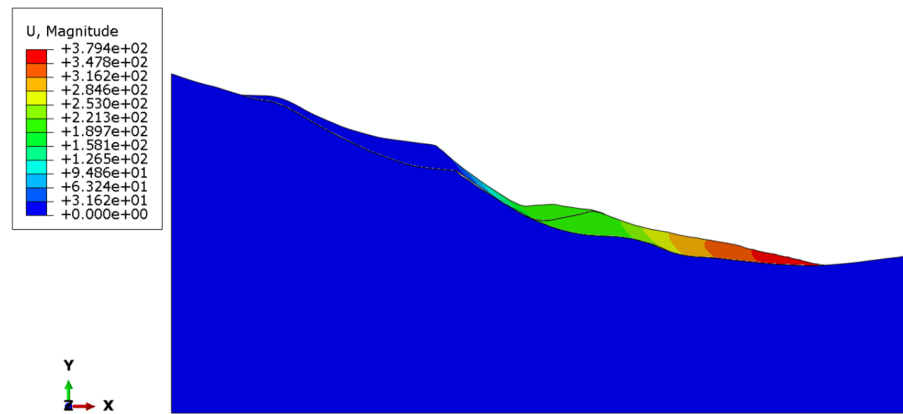
**(a)** Shared sliding surface



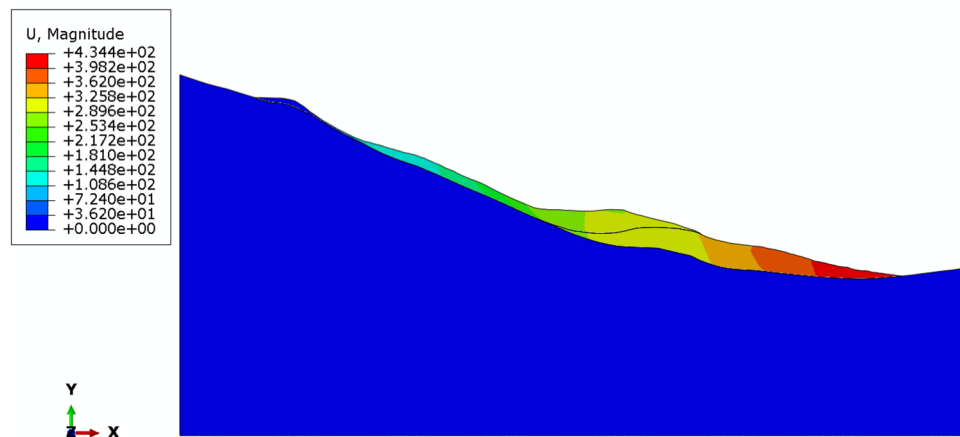
**(b)** Separate sliding surfaces



**Fig. 18** Final deposits for progressive failures with shared and separate sliding surfaces (unit: m)



**(a)** Progressive failure with separate sliding surfaces



**(b)** Progressive failure with shared sliding surface

**Sliding sequences**

Further calculations are conducted for the thrust-type landslides, as the existence of tensile cracks at the rear part and the increase of pore water pressure reduce the

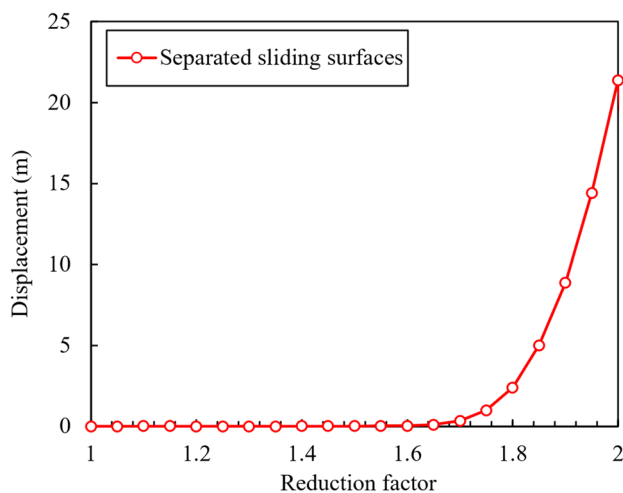
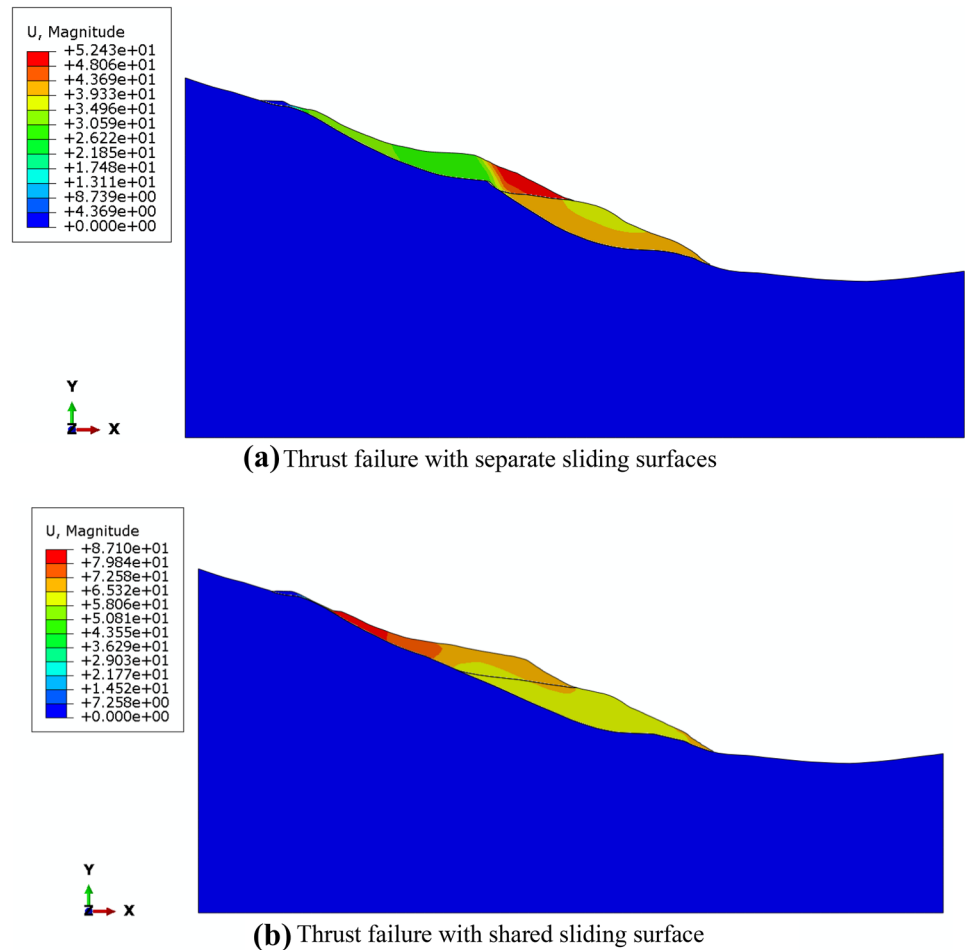


**Fig. 19** Strength reduction factors for the remaining part of the upper slide mass

normal effective stress under the effect of rainfall infiltration. This eventually leads to damping of the sliding resistance of the sliding surface, the process of which is triggered by setting the shear strength of the sliding surface underneath the upper sliding mass as the residual shear strength. For the thrust-type landslides, the movement of the upper sliding mass always pushes the lower mass as an overload. When the overload overwhelms the resistance of the lower mass, the lower mass will also fail, causing a chain of sliding events (Fig. 20). In that case, whether the two sliding masses share a sliding surface or not seems to be less important. The existence of the lower sliding mass essentially provides extra support to the upper sliding mass. Therefore, the final run-out distance of the masses (72 m) is significantly smaller than that of the retrogressive model (430 m). The comparison indicates that the failure of a retrogressive landslide is much more harmful than that of a thrust-type landslide in the multi-stage landslide events.

In combination of the effects of sliding surfaces and sequences, the most dangerous case is the retrogressive landslide complex sharing common sliding surfaces. The

**Fig. 20** Final deposits for thrust failures with shared and separate sliding surfaces (unit: m)



majority of the massive landslides in Three Gorges Reservoir area are retrogressive landslides with separate sliding surfaces, which may not be as harmful as speculated before.

## Conclusions

In this paper, a three-dimensional numerical model of the Huangtupo landslide in the Three Gorges Reservoir was established with the Arbitrary Lagrangian–Eulerian (ALE) method through the digital elevation model. The reliability of the ALE method was verified through the slurry runout induced by a dam break. The strength reduction method (SRM) was incorporated in the ALE method to assess the sliding risk of the Huangtupo landslide by a reverse analysis of the shear strength parameters of the materials in the sliding zone. The main conclusions are drawn as follows:

The strength parameters are required to be reduced to 89% and 86% of their initial values for failure to occur in the No. 1 and the No. 2 sliding masses, respectively. This indicates that the No. 1 sliding mass loses stability at an earlier time than the No. 2 sliding mass, which is attributed

to water-induced deterioration. The maximum displacements and velocities of the No. 1 and the No. 2 sliding masses mainly occur at the leading edge with final run-out distances of approximately 105 m and 175 m, respectively. The sliding velocities for the No. 1 and the No. 2 sliding masses are up to 2.97 m/s and 9.25 m/s, respectively. The volume of the No. 1 and the No. 2 sliding masses falling into the waterway of the reservoir area (below 175 m water level) are approximately 9.39 million and 9.18 million m<sup>3</sup>, respectively. A large extensional deformation occurs in the leading edge of the overlapping No. 3 and No. 4 sliding masses after the two riverside sliding masses collapse, in which significant plastic strains are similarly distributed. The stability coefficients of the No. 3 and the No. 4 sliding masses do not decrease sharply and remain stable as a whole, indicating that the catastrophic landslide disaster of the overall collapse in the Huangtupo landslide induced by the failure of No. 1 and No. 2 sliding masses might be unlikely.

For multi-stage landslides with separate sliding surfaces, the collapse of the lower sliding mass will not necessarily cause an overall failure of the upper sliding mass. In contrast, when the sliding masses have a shared sliding

surface, the failure of lower sliding mass directly leads to a successive overall sliding of the adjacent upper sliding mass. This highlights that a common sliding surface between the upper and lower sliding masses is important for the overall sliding of multi-stage landslides. For the thrust-type landslides, the movement of the upper sliding mass always pushes the lower mass as an overload, which is likely to cause the failure of the lower sliding mass, resulting in a chain of sliding events. As the existence of the lower sliding mass essentially provides extra support to the upper sliding mass, the destructiveness of a thrust-type landslide is significantly smaller than a retrogressive landslide in the multi-stage landslide events.

For the purpose of minimising the impact imposed by landslide on human, damage to property, and loss of life, early warning system has been constructed on the Huangtupo landslide by taking advantages of Global Navigation Satellite System (GNSS), InSAR, clinometers, and local displacement sensors. Moreover, special attention should be paid to the monitoring of strength degradation of rock/soil materials within the hydro-fluctuation zone. However, uncertainties surrounding the applicability of these monitoring methods persist as slope failure often occurs at unpredicted locations. Through the above numerical calculations, the ALE has been shown as an efficient and reliable tool to simulate the movement process of the slope under different conditions. Potential failure patterns and the corresponding consequence of the slope failure can be reasonably predicted. This is of considerable significance for those landslide complexes that may cause massive destructions. Even so, the uncertainties associated with the input parameters of the numerical model and accordingly with the predicted results should be considered as the limitation of the ALE simulations.

**Funding** This paper was supported by the National Natural Science Foundations of China (Grant Nos. 51909248, 41972298) and the Chongqing Geological Disaster Prevention and Control Center of China (Grant No. 20C0023).

**Data availability** The data that support the findings of this study are available from the corresponding author upon reasonable request.

## Declarations

**Competing interests** The authors declare no competing interests.

## References

- Abaqus G (2011) Abaqus 6.11. Dassault Systemes Simulia Corporation, Providence, RI, USA
- Alonso EE, Pinyol NM (2016) Numerical analysis of rapid drawdown: applications in real cases. *Water Sci Eng* 9(3):175–182
- Aubram D, Rackwitz F, Wriggers P, Savidis SA (2015) An ALE method for penetration into sand utilizing optimization-based mesh motion. *Comput Geotech* 65:241–249
- Chen XP, Zhu HH, Huang JW, Liu D (2016) Stability analysis of an ancient landslide considering shear strength reduction behavior of slip zone soil. *Landslides* 13(1):173–181
- Cojean R, Cai Y (2011) Analysis and modeling of slope stability in the Three-Gorges Dam reservoir (China) — The case of Huangtupo landslide. *J Mt Sci* 8:166
- Della Seta M, Martino S, Scarascia Mugnozza G (2013) Quaternary sea-level change and slope instability in coastal areas: insights from the Vasto Landslide (Adriatic coast, central 304 Italy). *Geomorphology* 201:462–478
- Deng Q, Zhu Z, Cui Z, Wang X (2000) Mass rock creep and landsliding on the Huangtupo slope in the reservoir area of the Three Gorges Project. *Yangtze River Eng Geol* 58(1):67–83
- Di Y, Yang J, Sato T (2007) An operator-split ALE model for large deformation analysis of geomaterials. *Int J Numer Anal Methods Geomech* 31(12):1375–1399
- Dijkstra J, Broere W, Heeres OM (2011) Numerical simulation of pile installation. *Comput Geotech* 38(5):612–622
- Dong Y (2020) Reseeding of particles in the material point method for soil-structure interactions. *Comput Geotech* 127:103716
- Dong Y, Wang D, Cui L (2019) Assessment of depth averaged method in analysing runout of submarine landslide. *Landslides* 17:543–555
- Dong Y, Cui L, Zhang X (2022) Multiple-GPU for three dimensional MPM based on single-root complex. *Int J Numer Meth Eng* 123:1481–1504
- Du J, Yin K, Lacasse S (2013) Displacement prediction in colluvial landslides, Three Gorges Reservoir, China. *Landslides* 10:203–218
- Fan N, Jiang J, Dong Y, Guo L, Song L (2022) Approach for evaluating instantaneous impact forces during submarine slide-pipeline interaction considering the inertial action. *Ocean Eng* 245:110466
- Greene HG, Murai LY, Watts P, Maher NA, Fisher MA, Paull CE (2008) Submarine landslides in the Santa Barbara Channel as potential tsunami sources. *Nat Hazard* 6:63–88
- Griffiths DV, Lane PA (1999) Slope stability analysis by finite elements. *Géotechnique* 49(3):387–403
- Guo X, Nian T, Fu C, Zheng D (2023b) Numerical investigation of the landslide cover thickness effect on the drag forces acting on submarine pipelines. *J Waterw Port Coast Ocean Eng* 149:2
- Guo X, Stoesser T, Zheng D, Luo Q, Liu X, Nian T (2023a) A methodology to predict the run-out distance of submarine landslides. *Comput Geotech* 153:105073
- Hirt CW, Amsden AA, Cook JL (1974) An Arbitrary Lagrangian-Eulerian computing method for all flow speeds. *J Comput Phys* 14:227–253
- Hu X, Zhou C, Xu C, Liu D, Wu S, Li L (2019) Model tests of the response of landslide-stabilizing piles to piles with different stiffness. *Landslides* 16:2187–2200
- Huang D, Gu D, Song Y, Cen D, Zeng B (2018) Towards a complete understanding of the triggering mechanism of a large reactivated landslide in the Three Gorges Reservoir. *Eng Geol* 238:36–51
- Huang F, Huang J, Jiang S, Zhou C (2017) Landslide displacement prediction based on multivariate chaotic model and extreme learning machine. *Eng Geol* 218:173–186
- Jian W, Wang Z, Yin K (2009) Mechanism of the Anlesi landslide in the Three Gorges Reservoir. *China Eng Geol* 108(1–2):86–95
- Kasai M, Ikeda M, Asahina T, Fujisawa K (2009) LiDAR-derived DEM evaluation of deep seated landslides in a steep and rocky region of Japan. *Geomorphology* 113(1–2):57–69
- Krone RB, Wright VG (1987) Laboratory and numerical study of mud and debris flow. Report 1 and 2 for Department of Civil Engineering, University of California, Davis
- Luo S, Huang D (2020) Deformation characteristics and reactivation mechanisms of the Outang ancient landslide in the Three Gorges Reservoir, China. *Bull Eng Geol Environ* 79:3943–3958

- Miao FS, Wu YP, Xie YH, Li LW, Li J, Huang L (2019) Influence of permeation effect on the microfabric of the slip zone soils: a case study from the Huangtupo landslide. *J Mt Sci* 16(6):1231–1243
- Miao FS, Wu YP, Torok A, Li L, Xue Y (2022) Centrifugal Model Test on a Riverine Landslide in the Three Gorges Reservoir Induced by Rainfall and Water Level Fluctuation 13(3):101378
- Matsui T, San KC (1992) Finite element slope stability analysis by shear strength reduction technique. *Soils Found* 32(1):59–70
- Nazem M, Carter J, Airey D (2009) Arbitrary Lagrangian-Eulerian method for dynamic analysis of geotechnical problems. *Comput Geotech* 36(4):549–557
- People's Republic of China National Standard (2016) Code for geological Investigation of landslide prevention (GB T 32864–2006). China Standardization Press, Beijing
- Soga K, Alonso E, Yerro A, Kumar K, Bandara S (2016) Trends in large-deformation analysis of landslide mass movements with particular emphasis on the material point method. *Géotechnique* 66(3):248–273
- Song H, Cui W (2016) A large-scale colluvial landslide caused by multiple factors: mechanism analysis and phased stabilization. *Landslides* 13(2):321–335
- Tang H, Li C, Hu X, Su A, Wang L, Wu Y, Criss R, Xiong C, Li Y (2015) Evolution characteristics of the Huangtupo landslide based on in situ tunneling and monitoring. *Landslides* 12(3):511–521
- Tomás R, Li Z, Lopez-Sanchez JM, Liu P, Singleton A (2016) Using wavelet tools to analyse seasonal variations from InSAR time-series data: a case study of the Huangtupo landslide. *Landslides* 13(3):437–450
- Wang D, Randolph MF, White DJ (2013) A dynamic large deformation finite element method based on mesh regeneration. *Comput Geotech* 54:192–201
- Wang F, Zhang Y, Huo Z (2004) The July 14, 2003. Qianjiangping landslide, Three Gorges Reservoir, China. *Landslides* 1(2):157–162
- Wang JJ, Liang Y, Zhang HP, Wu Y, Lin X (2014) A loess landslide induced by excavation and rainfall. *Landslides* 11(1):141–152
- Wang J, Wang S, Su A, Xiang W, Xiong C, Blum P (2021) Simulating landslide-induced tsunamis in the Yangtze River at the Three Gorges in China. *Acta Geotech* 16(8):2487–2503
- Wang S, Wang J, Wu W, Cui D, Su A, Xiang W (2020) Creep properties of clastic soil in a reactivated slow-moving landslide in the Three Gorges Reservoir Region. *China Eng Geol* 267:105493
- Wang S, Wu W, Wang J, Yin Z, Cui D, Xiang W (2018) Residual-state creep of clastic soil in a reactivated slow-moving landslide in the Three Gorges Reservoir Region. *China Landslides* 15(12):2413–2422
- Wen B, Chen H (2007) Mineral compositions and elements concentrations as indicators for the role of groundwater in the development of landslide slip zones: a case study of large-scale landslides in the Three Gorges Area in China. *Earth Sci Front* 14(6):98–106
- Xia M, Ren GM, Zhu SS, Ma XL (2015) Relationship between landslide stability and reservoir water level variation. *Bull Eng Geol Env* 74(3):909–917
- Xu S, Niu R (2018) Displacement prediction of Baijiabao landslide based on empirical mode decomposition and long short-term memory neural network in the Three Gorges area, China. *Comput Geosci* 111:87–96
- Yin Y, Wang H, Gao Y, Li X (2010) Real-time monitoring and early warning of landslides at relocated Wushan Town, the Three Gorges Reservoir, China. *Landslides* 7:339–349
- Young AP (2015) Recent deep-seated coastal landsliding at San Onofre State Beach, California. *Geomorphology* 228:200–212
- Yu X, Wu Y (1996) A study on the mechanism of Sandaogou Landslide in urban area of Badong County. *J Eng Geol* 4(1):1–7
- Yuan W, Liu K, Zhang W, Dai B, Wang Y (2020) Dynamic modeling of large deformation slope failure using smoothed particle finite element method. *Landslides* 17:1591–1603
- Zhang W, Zhong Z, Peng C, Yuan W, Wu W (2021) GPU-accelerated smoothed particle finite element method for large deformation analysis in geomechanics. *Comput Geotech* 122:103856
- Zheng J, Hossain MS, Wang D (2018) Estimating spudcan penetration resistance in stiff-soft-stiff clay. *J Geotech Geoenviron Eng ASCE* 144(3):04018001
- Zheng J, Wang D (2019) Numerical investigation of spudcan-footprint interaction in non-uniform clays. *Ocean Eng* 188:106295
- Zienkiewicz OC, Humpheson C, Lewis RW (1975) Associated and non-associated viscoplasticity and plasticity in soil mechanics. *Géotechnique* 25(4):671–689

Springer Nature or its licensor (e.g. a society or other partner) holds exclusive rights to this article under a publishing agreement with the author(s) or other rightsholder(s); author self-archiving of the accepted manuscript version of this article is solely governed by the terms of such publishing agreement and applicable law.